Automatic Identification of Retinal Arteries and Veins From Dual-Wavelength Images Using Structural and Functional Features

Harihar Narasimha-Iyer, *Member, IEEE*, James M. Beach, Bahram Khoobehi, and Badrinath Roysam*, *Member, IEEE*

***Abstract*—This paper presents an automated method to identify arteries and veins in dual-wavelength retinal fundus images recorded at 570 and 600 nm. Dual-wavelength imaging provides both structural and functional features that can be exploited for identification.**

The processing begins with automated tracing of the vessels from the 570-nm image. The 600-nm image is registered to this image, and structural and functional features are computed for each vessel segment. We use the relative strength of the vessel central reflex as the structural feature. The central reflex phenomenon, caused by light reflection from vessel surfaces that are parallel to the incident light, is especially pronounced at longer wavelengths for arteries compared to veins. We use a dual-Gaussian to model the cross-sectional intensity profile of vessels. The model parameters are estimated using a robust M-estimator, and the relative strength of the central reflex is computed from these parameters. The functional feature exploits the fact that arterial blood is more oxygenated relative to that in veins. This motivates use of the ratio of the vessel optical densities (ODs) from images at oxygen-sensitive and oxygen-insensitive wavelengths ($\mathrm{ODR} = \mathrm{OD}_{600}/\mathrm{OD}_{570}$) as a functional indicator. Finally, the structural and functional features are combined in a classifier to identify the type of the vessel. We experimented with four different classifiers and the best result was given by a support vector machine (SVM) classifier.

With the SVM classifier, the proposed algorithm achieved true positive rates of 97% for the arteries and 90% for the veins, when applied to a set of 251 vessel segments obtained from 25 dual wavelength images. The ability to identify the vessel type is useful in applications such as automated retinal vessel oximetry and automated analysis of vascular changes without manual intervention.

***Index Terms*—Automated image analysis, automatic identification, retinal oximetry, structural and functional features, vessel profile modeling, vessel type.**

Manuscript received October 12, 2005; revised April 16, 2006. The Rensselaer component of this research was supported in part by the National Science Foundation (NSF) under Experimental Partnerships Grant EIA-0000417, the Center for Subsurface Sensing and Imaging Systems, under the Engineering Research Centers Program of the National Science Foundation (Award Number EEC-9986821). The team at the Institute for Technology Development and LSU acknowledges support from the NIH: EY14776 (Photon Industries, Inc.), EY012887, EY02377, and an unrestricted grant to LSU from Research to Prevent Blindness. *Asterisk indicates corresponding author.*

H Narasimha-Iyer is with Carl Zeiss Meditec, Dublin, CA 94568 USA (e-mail: harihar.n.iyer@gmail.com).

J. M. Beach is with the LSU Eye Center, LSU Health Sciences Center, New Orleans, LA 70112 USA and also with the Institute for Technology Development, Stennis Space Center, MS 39529 USA (e-mail: jbeach@iftd.org).

B. Khoobehi is with the LSU Eye Center, LSU Health Sciences Center, New Orleans, LA 70112 USA (e-mail: bkhoob@lsuhsc.edu).

*B. Roysam is with Rensselaer Polytechnic Institute, JEC 7010, 110 8th Street, Troy, NY 12180-3590 USA (e-mail: roysam@ecse.rpi.edu).

Color versions of one or more of the figures in this paper are available online at http://ieeexplore.ieee.org.

Digital Object Identifier 10.1109/TBME.2007.900804

I. Introduction

RETINAL vessels provide important indicators for clinical diagnosis and treatment of eye diseases. In diseases such as diabetes mellitus, early indications of retinal complications include abnormality of the blood vessels [1]. Changes in retinal blood vessels are also associated with hypertension [2] and other cardio-vascular diseases [3]. Arteries and veins are affected differently under disease conditions. For example, tortuosity changes in arteries and veins are very different during progression of retinopathy. Also, certain lesions are specific to the vessel type: focal narrowing for arteries and beading for veins. Also, while looking at vascular changes, the changes associated with arteries and veins need to be interpreted differently. For instance, in an application that measures the change in width of vessels, it would be advantageous to be able to identify the type of vessel that is undergoing the change. Another application where arteries and veins need to be considered separately is retinal vessel oximetry. Recently, algorithms have been described to automate measurement of the blood oxygen saturation from blood vessels and to analyze its changes over time [4]. In applications like this, it is of interest to identify the arteries and veins automatically to enable the analysis of changes in each type of vessel separately.

Though many methods have been proposed in the literature to segment retinal blood vessels, there has not been much published prior work on automatically identifying arteries and veins from retinal images. Yu *et al.* [5] used the criteria that arteries are lighter than veins and used intensity thresholding of pixels at a certain distance from the optic disk to label the vessels as arteries and veins. Akita and Kuga [6] identified the vessel types by initial labeling followed by relaxation labeling. They also used the intensity difference between arteries and veins as indicator and labeled the brighter and darker segments as artery and vein respectively. These methods did not try to model the cross-sectional profile of the vessel and hence may be prone to errors when the intensities are comparable. Grisan *et al.* [7] described a method for classifying retinal vessels in a concentric zone around the optic disk using the color information. A method that models the vessel cross-sectional profile was described by Li *et al.* in [8]. They modeled the cross-sectional intensity profiles of vessels by a piecewise dual-Gaussian model and estimated the model parameters using a least-squares fitting procedure. A minimum distance classifier based on the Mahalanobis distance was then used to differentiate between the

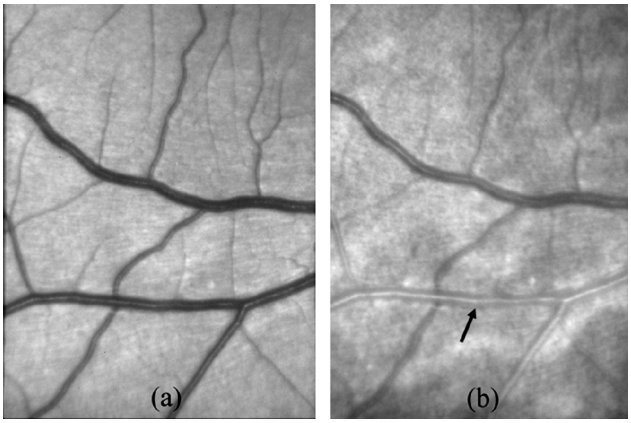

Fig. 1. Dual wavelength images: (a) 570-nm image showing higher contrast between the vessels and the background; (b) 600-nm image, showing lower contrast. The artery (indicated by arrow) can be seen to have a strong central reflex characteristic.

vessel types using features derived from the estimated parameters. Though this system was shown to have good classification performance, one drawback in using the least squares procedure would be the effect outliers would have on the estimation of the parameters. Clinical retinal images can be noisy [9], and in order to be robust to such noise, we need to incorporate robust procedures while estimating the intensity parameters.

In many cases, the intensity profile alone is insufficient to differentiate between arteries and veins, since the intensity distributions might be similar. A way to solve this problem is to use a functional feature which represents the functionality of the vessel. In this paper, we propose a novel approach, which uses structural as well as functional features to identify the vessel type from dual wavelength images, obtained at 570 and 600 nm. The 600-nm image is sensitive to changes in the percentage of systemic HbO_2 (oxygenated haemoglobin) present in the blood [10], while the 570-nm image is insensitive to HbO_2 change. Fig. 1 shows two images acquired simultaneously at 570 and 600 nm. The 570-nm image has higher contrast between the blood vessels and the background than does the image at 600 nm, where differential contrast between the artery and vein comes from the higher and lower HbO_2 content in each vessel. Retinal vessels also exhibit a strong reflection along their centerline (central vessel reflex) which is more pronounced in arteries and than veins, and is stronger at longer wavelengths. This effect is believed to result from specular reflection at the interface between the retina and vitreous (internal limiting membrane). Tissue properties specific to the arterial smooth muscle layer could be responsible for differences in the reflexes in the two vessel types. We exploit this information from two wavelengths and propose a system that automatically segments the vessels, robustly extracts structural (based on the intensity cross-section) and functional features (based on the optical densities) and recognizes the vessel type.

II. Background

In this paper, we bring together different aspects of retinal image analysis which include vessel segmentation, vessel modeling and retinal vessel oximetry. Here we will briefly describe some of the previous work on each of these areas and mention how they are related to our work where applicable.

Vessel segmentation from retinal images is a problem that has been widely studied in the literature [11]–[23]. The main methods can be classified into four categories: approaches based on adaptive filtering or segmentation [11]–[14], vessel tracking [15]–[18], mathematical morphology [19], [20], and classification [21], [22]. For segmenting vessels from the 570-nm image, we use the tracing algorithm of Can *et al.* [16], [17]. This algorithm is based on recursively tracking the vessels starting from initial seed-points, using directional templates. Each directional template is designed to give the maximum response for an edge oriented in a particular direction. Around each candidate vessel point, the templates are applied on either side of the point at varying distances. The edges are marked at points that yield the maximum response for the templates. The algorithm takes a step in the direction of maximum response and the procedure is repeated at the new point. Retinal features such as branching and cross-over points of the vessels are estimated by this algorithm once the vessels are segmented. This algorithm is very fast and prioritized versions have been used for real time feature extraction and registration at frame rates of 30 frames/s [23], [24]. The tracing algorithm is based on finding the edges of the vessels and as such does not give detailed information regarding the exact vessel profile. The structural feature we are proposing to use in this paper needs this detailed information. A robust vessel detection method was described in [9] to detect vessels from extremely noisy images. We use the robust estimation procedure described there to estimate the parameters of the cross-sectional intensity profile of the vessels.

Several models have been proposed for the cross sectional intensity profile of retinal vessels. These model include the Gaussian profile [11], [25], the second-order derivative Gaussian suggested by Gang *et al.* [26], [27], the cubic spline profile by Pedersen *et al.* [28], the parallel edge model by Can *et al.* [15], [16] and Vermeer *et al.* [29], the piece-wise dual-Gaussian proposed by Li *et al.* [8], and the model based on ellipsoidal projections described by Pappas and Lim [30]. An analysis of different vessel profiles is described by Roberts [31]. In this paper, we will be modeling the central reflex characteristics in the vessel using the twin-Gaussian proposed by Gao *et al.* [32]. This model has two terms that are additive and help to model the central reflex adequately. Also, the simplicity of the model lends itself to the robust estimation framework to be described later.

Many advances and refinements in technique for retinal oximetry have been made over the past four decades [4], [33], [34]. Hickham *et al.* [33], [34] were the first to report studies of retinal oxygenation in man by noninvasive measurements, using photographic methods to record vessel optical density (OD) at oxygen-sensitive and insensitive wavelengths, and ratio analysis to obtain relative measures of oxygen saturation. Laing and Cohen [35] extended this method by showing that blood saturation varied linearly with the ratio over physiological and hypoxic ranges of saturation. Delori developed a three wavelength oximetry method to obtain absolute oxygen saturation values from single vessel segments [36]. A method to perform

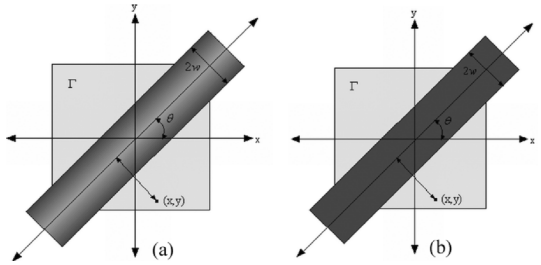

Fig. 2. Illustrating the window Γ used for estimating the model parameters for two cases of interest. (a) Vessel with central reflex passing through the origin. (b) Vessel without central reflex passing through the origin. Depending on the position of the pixel with respect to the origin, it is expected to have a particular intensity given by the vessel profile model illustrated in Fig. 3.

retinal vessel oximetry by spectroscopic recording was introduced by Schweitzer *et al.* [37]. Jensen *et al.* [38] and Critten *et al.* [39] have employed the ratio technique successfully to measure oxygen saturation changes in retinal vessels. Recently, Khoobehi *et al.* [40] employed hyperspectral imaging to monitor the relative spatial changes in retinal oxygen saturation of the retina and optic disc tissue in the monkey. Uzumcu *et al.* [41] obtained measurements at 6 wavelengths and estimated the parameters related to the oxygen saturation using an iterative algorithm. A scanning laser ophthalmoscope which images at 4 wavelengths was used by Smith *et al.* [42], [43]. In this paper, we use the method described by Beach *et al.* [10] that is based on ratiometric measurements and digital imaging techniques to simultaneously record oxygen-sensitive and insensitive images at two wavelengths.

In the subsequent sections, we will describe how the structural and functional features are estimated and how the features are used to identify arteries and veins.

III. Estimating the Structural Feature

Arteries exhibit a strong central reflex phenomenon in the 600-nm image, while the central reflex is relatively low for veins. The strength of the central reflex could be used as a feature to identify the vessel type. In order to use the information from the central reflex, we should be able to extract the parameters of the intensity profile of a vessel.

Suppose we are interested in estimating the parameters of the vessel cross section at a particular point, which is assumed to be the coordinate origin without loss of generality. The two cases of interest here are a vessel with central reflex and a vessel without a central reflex. These two cases are illustrated in Fig. 2. The vessel segments can be assumed to be locally linear, with a width $2w$, with parallel edges along a particular orientation θ over the window Γ. The grayscale cross-sectional profile of the vessel is modeled by $f\left(r_\theta(x,y),\Theta\right)$, where $r_\theta(x,y)$ is the distance from the vessel centerline, and Θ is the parameter vector for the intensity profile, $f(.)$.

As mentioned in the previous section, many models have been described for the cross-sectional intensity profile. The model proposed by Gao *et al.* [32] is given by

$$f(r_\theta(x,y),\Theta) = \lambda_1 - (\lambda_1-\lambda_2)\exp\left(-\frac{r_\theta^2(x,y)}{2\sigma_1^2}\right) + \lambda_3 \exp\left(-\frac{r_\theta^2(x,y)}{2\sigma_2^2}\right) \quad (1)$$

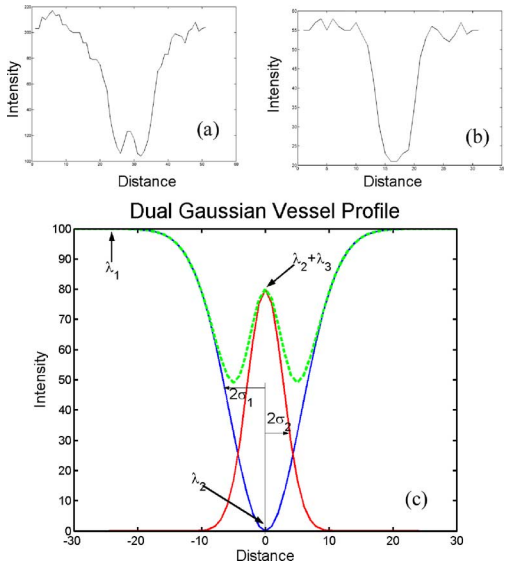

Fig. 3. Vessel cross-sectional profiles. Panels (a) and (b) show sample cross-sectional profiles of vessels without and with central reflex respectively. Panel (c) illustrates the dual-Gaussian model. The curve in blue is the single Gaussian model. The curve in red is the reflex term. The two curves add to give the vessel profile displayed in green. To generate the example profile in the figure, the following parameters were used. $\lambda_1 = 100, \lambda_2 = 0, \lambda_3 = 80, \sigma_1 = 4$ and $\sigma_2 = 2$.

where $f\left(r_\theta(x,y),\Theta\right)$ is the intensity profile and $\Theta = \{\lambda_1,\lambda_2,\lambda_3,\sigma_1,\sigma_2\}$ are the parameters that describe the relative intensities, total width of the vessel and width of the central reflex, respectively. Specifically, for vessels without the central reflex, λ_1 is the background intensity, and $(\lambda_1-\lambda_2)$ is the relative contrast of the vessel against the background. In the case of a vessel with central reflex, λ_2 decides how fast the intensity is falling off from the edges and towards the central reflex. λ_3 is the multiplier for the Gaussian that models the central reflex. It is related to the strength of the central reflex and the peak central reflex is given by $\lambda_2+\lambda_3$, which occurs at $r_\theta(x,y)=0$, the center of the vessel. The parameters, σ_1 and σ_2 are related to the width of the vessel and the width of the reflex. Fig. 3(a) and 3(b) show examples of intensity profiles of vessels without and with central reflex. Fig. 3(c) illustrates the dual Gaussian model with the associated parameters.

We now describe the estimation procedure for the parameters of the dual-Gaussian model in (1). Let $s(x_i,y_i)$ be the intensity of the image at location (x_i,y_i). We can fit the model to the intensities inside the window Γ, by minimizing a function that represents how well the model fits the data. Let the difference between the measured intensity at point (x_i,y_i) and the intensity predicted by the model be denoted by

$$\gamma_i = s(x_i,y_i) - f\left(r_\theta(x_i,y_i),\Theta\right). \quad (2)$$

The sum of squares of the error at each pixel inside the window Γ gives a measure of how well the model fits the data and is given by

$$\phi(\Theta) = \sum_{i=1}^{n} \gamma_i^2. \quad (3)$$

Here, index i denotes the pixel number within the window Γ. The least-squares solution for (3) can be found as

$$\hat{\Theta} = \arg\min_{\{\Theta\}} \{\phi(\Theta)\}. \tag{4}$$

The least squares solution in (4) can be influenced by outliers in the data and hence we use the robust M-Estimator [44], [45] to estimate the parameters. One way of robustly estimating the parameters is to use a robust loss function, ρ that has a less than quadratic growth rate as a function of the residue. The robust objective function to minimize is now given by

$$\phi^{\mathrm{R}}(\Theta) = \sum_{i=1}^{n} \rho\left(\frac{\gamma_i}{\sigma_d}\right) \tag{5}$$

where σ_d is called the scale and is a measure of the dispersion of the residuals. Many alternatives have been suggested for the robust loss function such as the Beaton-Tukey [46] and the Cauchy [47]. In this paper, we use the Cauchy loss function and it is given by

$$\rho_C(t) = \frac{C^2}{2} \log\left[1 + \left(\frac{t}{C}\right)^2\right] \tag{6}$$

where C is a parameter that controls the weighting given to inliers and outliers.

The model parameters that we seek are the values that minimize the robust objective function in (5) as

$$\hat{\Theta} = \arg\min_{\{\Theta\}} \left\{\phi^{\mathrm{R}}(\Theta)\right\}. \tag{7}$$

Assuming we know the direction (θ) of the vessel from tracing the vessel at 570 nm, the parameter vector of interest is given by

$$\Theta = [\,\lambda_1 \quad \lambda_2 \quad \lambda_3 \quad \sigma_1 \quad \sigma_2\,]^T. \tag{8}$$

The minimization of (7) can be done using a nonlinear optimization framework [9]. The iterative procedure consists of starting from an initial estimate of the parameters and then updating them until a convergence criterion is reached. The update equation is given by

$$\Theta^{k+1} = \Theta^k + \delta^k \tag{9}$$

where Θ^k is the value of the parameters and δ^k is the update term at iteration k. We use the iteratively reweighted least squares (IRLS) scheme to do the minimization, the details of which are presented in [9].

Once the parameter vector $\hat{\Theta}$ has been robustly estimated as described, we form a structural feature at a point of the vessel as

$$f_{struc} = \frac{\hat{\lambda}_2 + \hat{\lambda}_3}{\hat{\lambda}_1}. \tag{10}$$

As can be seen from Fig. 3, this ratio is a measure of the strength of the central reflex relative to the background intensity. We expect this feature to be higher for arteries and lower for veins. A vessel segment is defined as a set of vessel center line points. The vessel segments with their associated center line points are obtained from the tracing algorithm. For estimating the structural feature for a vessel segment, we take the average of f_{struc} over the vessel centerline points on this segment and use that as the structural feature for the entire segment.

IV. Estimating the Functional Feature

In order to capture the functionality of the vessel, we use a quantity called ODR that is inversely proportional to the $\mathrm{HbO_2}$ saturation in the blood [4]. Usually, arteries have a low ODR value and veins have a relatively larger ODR value. As the first step in calculating the ODR for each vessel segment, we should find the OD value for the segments at the two wavelengths (570 and 600 nm). The method for calculating this is described later.

The images at 570 and 600 nm are first registered to each other using the dual bootstrap ICP algorithm [48]. The image at 570 nm, which has greater contrast, is then traced using the exploratory tracing algorithm [16], [17] as described before. The algorithm finds the vessel centerlines as well as the width and direction at each centerline point. The OD for a segment can then be calculated by finding the minimum intensity inside the vessel and the average outside intensity. This idea is made precise below. We will use vector notation for the image coordinate points in this section to simplify the equations. Let $\vec{p}^k$ represent the kth centerline point in a vessel segment and let $\vec{r}^k$ and $\vec{l}^k$ denote the right and left boundary points. The minimum intensity inside the vessel at $\vec{p}^k$ is given by

$$I_{\mathrm{in}}(\vec{p}^k) = \arg\min_t \{I(t\vec{r}^k + (1-t)\vec{l}^k)\} \tag{11}$$

where $I(\vec{m})$ is the image intensity at point $\vec{m}$ and t is a parameter that varies from 0 to 1. Equation (11) finds the point with minimum intensity along the straight line joining $\vec{r}^k$ and $\vec{l}^k$. Extra-vascular light reflection at point $\vec{p}^k$ is measured from points lying at one vessel diameter distance on either side of the vessel boundary. It is given by:

$$I_{\mathrm{out}}(\vec{p}^k) = \frac{1}{2}\{I(\vec{r}^k + Du_\perp^k) + I(\vec{l}^k - Du_\perp^k)\} \tag{12}$$

where D is the diameter of the vessel at that point and $u_\perp^k$ is the unit vector in the direction perpendicular to the local direction of the vessel at $\vec{p}^k$. In order to reduce the effect of noise, we can use a local average to calculate the extra vascular light reflection. Equation (12) can be modified to

$$I_{\mathrm{out}}(\vec{p}^k) = \frac{1}{2}\{\mathrm{Avg}_w[\vec{r}^k + Du_\perp^k] + \mathrm{Avg}_w[\vec{l}^k - Du_\perp^k]\} \tag{13}$$

where

$$\mathrm{Avg}_w[\vec{p}] = \frac{1}{(2w+1)^2} \sum_{i=-w}^{w} \sum_{j=-w}^{w} I(p_x + i, p_y + j). \tag{14}$$

As described in [4], the OD can be calculated in two ways for the same segment. Here we use the method that is robust to illumination gradients across the image. The OD is calculated for each centerline point in the trace segment and then the individual

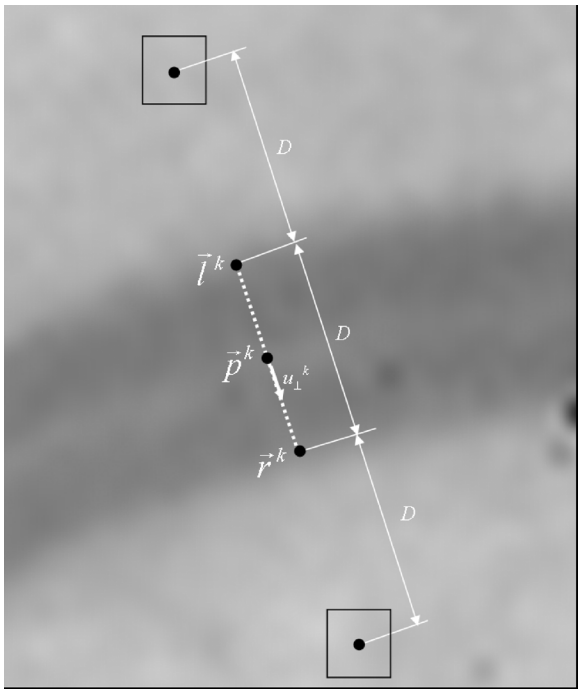

Fig. 4. Illustrating the OD calculation method. The blue dots on the vessel indicate the centerline point $\vec{p}^k$, the left boundary point, $\vec{l}^k$ and the right boundary point, $\vec{r}^k$. The unit vector in the direction perpendicular to the vessel orientation is denoted by $u_\perp^k$ and D is the diameter of the vessel at $\vec{p}^k$. The two red dots on the outside of the vessel indicate the centroids of the neighborhoods over which the average extra-vascular reflection is measured. The white dot represents the minimum-intensity point inside the vessel.

ODs are averaged to obtain the overall OD for the segment. The OD at centerline point p^k from the 570-nm image is given by

$$\mathrm{OD}_{570}(\vec{p}^k) = \log_{10}\left(\frac{I_{\mathrm{out}}(\vec{p}^k)}{I_{\mathrm{in}}(\vec{p}^k)}\right) \tag{15}$$

and the average OD for segment i with M points is calculated as

$$\mathrm{OD}_{570,\mathrm{seg}}(i) = \frac{1}{M}\sum_{k=1}^{M}\mathrm{OD}(\vec{p}^k), \tag{16}$$

$$= \frac{1}{M}\sum_{k=1}^{M}\log_{10}\left(\frac{I_{\mathrm{out}}(\vec{p}^k)}{I_{\mathrm{in}}(\vec{p}^k)}\right). \tag{17}$$

The OD at 600 nm is also calculated using the same procedure and the OD ratio (ODR) for segment i is calculated as

$$\mathrm{ODR}_{\mathrm{seg}}(i) = \frac{\mathrm{OD}_{600,\mathrm{seg}}(i)}{\mathrm{OD}_{570,seg}(i)}. \tag{18}$$

Fig. 4 shows the illustration of how the OD is calculated for a segment. The ODR from each segment is used as the functional feature

$$f_{\mathrm{func}} = \mathrm{ODR}_{\mathrm{seg}}(i). \tag{19}$$

V. Classification

The features described above are now combined in a classifier to identify the type of the vessel. In order to find a good classifier, we tested the training set with four different classifiers namely: Nearest Neighbor, 5 Nearest Neighbor, Fisher Linear discriminant (FLD) and a support vector machine (SVM) classifier.

Nearest Neighbor (k-NN) classifiers are nonlinear classifiers where the label for a test sample is decided based on the labels of its "k" nearest neighbors in the training set. These classifiers are conceptually simple and give good performance when the data is clearly separable. We used values of $k = 1$ and $k = 5$ for classifying the test set. FLD analysis seeks a direction that is efficient for discriminating between the samples. We use the implementation in the PRTools Toolbox [49] for the k-NN and the FLD classifier.

SVMs are adaptive algorithms for classification and regression [50]. They have been used in a variety of applications including 3-D object recognition [51], speaker verification [52], face detection [53] and text classification [54]. This list is by far not complete and is only intended to highlight the diversity of the applications in which SVMs have been used. SVMs are based on structural risk minimization, which aims at minimizing the generalization error, which is the error made by the learning machine on data that is not seen during the training phase [49]. Hence, SVMs are found to perform well on data that is not in the training set.

Let $\{(u_1, v_1), (u_2, v_2), \ldots\ldots(u_N, v_N)\}$ be a training data set with u_i representing the classification features and v_i representing the binary class labels. The problem is then to design a classifier, $f(u)$ from the training data that can correctly determine the class label of an input pattern with feature vector u. In principle, a nonlinear SVM classifier maps the input feature vector u into a higher dimensional space H through an underlying nonlinear mapping $\Phi(u)$. Linear classification is then done in the mapped space. The SVM classification function can be written as

$$f_{\mathrm{svm}}(u) = w^T\Phi(u) + b \tag{20}$$

where w and b are parameters of the classifier and are determined from the training set.

A training sample (u_i, v_i) is called a support vector if $v_i f_{\mathrm{svm}}(u_i) \leq 1$. Denoting the kernel function by $K(a,b) = \Phi(a)^T\Phi(b)$, the kernel form of (20) can be written as

$$f_{\mathrm{svm}}(u) = \sum_{i=1}^{N_s}\alpha_i K(u, s_i) + b \tag{21}$$

where s_i are the support vectors and N_s is the number of support vectors. Equation (21) helps us to directly evaluate the decision function using $K(\cdot,\cdot)$.

In this paper, we use the SVM Matlab Toolbox provided by Anton Schwaighofer [55]. The radial basis function (RBF) is used as the kernel function and is given by

$$K(a,b) = \exp\left(-\frac{\| a-b \|^2}{2\sigma_{\mathrm{rbf}}^2}\right) \tag{22}$$

where σ_{rbf} is a parameter that controls the width of the kernel. This parameter is selected according to the method described in [56].

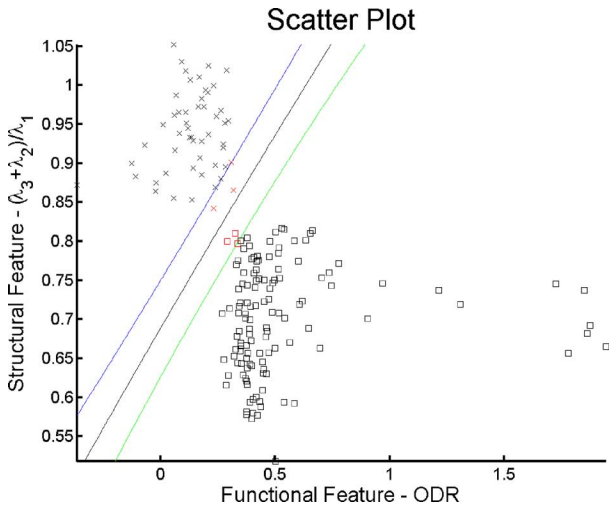

Fig. 5. Scatter plot of the structural and functional features, and the support vectors. The points shown as crosses are the arteries and the points shown as squares are the veins. The lines indicate the support vectors. A kernel width of 0.92 was used in this SVM.

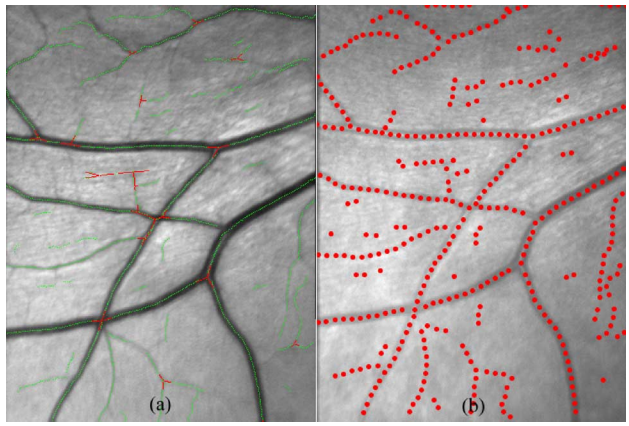

Fig. 6. Automatic selection of candidate points. (a) Results of the exploratory tracing algorithm on the 570-nm image. The centerline points are shown in green and the branching and cross-over points detected by the algorithm are shown in red. (b) Candidate points (shown in red) where the vessel profile is estimated robustly to find the structural feature. The points are overlaid on the 600-nm image.

A. *Experimental Validation Results*

The training and test image sets were both obtained from normal healthy volunteers at the Eye Center, Department of Ophthalmology at Louisiana State University Health Sciences Center in New Orleans, LA. Imaging methods were described previously [4], [10]. Briefly, with institutional review board approval, subject's right eyes were dilated with 1% tropicamide and 2.5% phenylephrine. Recordings of retinal vessels were made simultaneously at 570 and 600 nm using an image splitter attached to a fundus camera (Topcon) with a digital CCD camera positioned to record the images on each side of the sensor. Recordings included sites containing major vessels leaving the optic disc and distal sites containing smaller branches of the major vessels, where a prominent artery and vein were visible. Field of view was set to 50 degrees and illumination came from the internal strobe at either 30 and 50 Joules setting. The two views of the retina each contained approximately 360×512 pixels. The pixel resolution was 9 μm$\times$ 9 μm.

Five training images were selected with varying vessel profiles and points on arteries and veins were selected manually by a user. The training vectors were derived from these images and the different classifiers were trained using these features.

The rest of the images were processed to test the algorithms. The images obtained at 570 and 600 nm were first registered to each other. The 570-nm images were then traced using the exploratory algorithm described earlier to segment the vessels. Candidate locations to estimate the structural and functional features were selected from the vessel centerlines obtained in the earlier step. In order to reduce the number of estimation steps for a single segment, we sub-sampled the centerline points obtained from the 570-nm image and took every 5th centerline point as the candidate point. Fig. 6 illustrates the traces obtained on the 570-nm image and the automatically selected candidate points overlaid with red on the 600-nm image.

The vessel profile was robustly estimated at each of the candidate points to obtain the structural feature. The optical densities were obtained from both wavelengths and their ratio is formed to find the OD ratio (ODR). The vessel segments were then classified using the classifiers. Ground truth data was obtained from 25 dual wavelength images by manually picking significant vessels and indicating their types. A total of 251 vessel segments were identified and labeled in this manner. Since the structural features and functional features are not stable in small vessels, only vessel segments which were 8 pixel or more in width were considered. Also, only vessels whose type could be identified without any ambiguity were included in the ground truth. The results of automatic classification were compared against this ground truth data to validate the algorithm performance.

Since different segments have different lengths, a fair validation of the method in terms of it performance will be to consider the length of the segments which are being classified. For example, the true positive rate for arteries, $\mathrm{TP}_{\mathrm{artery}}$ is defined as

$$\mathrm{TP}_{\mathrm{artery}} = \frac{\sum_j l_a(j)}{\sum_i l_a(i)} \tag{23}$$

where $l_a(i)$ refers to the length of the ith artery segment. The index j in the numerator corresponds to the index of the arteries that have been classified correctly. The misclassification rate is defined as

$$\mathrm{MC}_{\mathrm{artery}} = \frac{\sum_k l_a(k)}{\sum_i l_a(i)} = (1 - \mathrm{TP}_{\mathrm{artery}}). \tag{24}$$

The index k in the numerator corresponds to the index of the arteries that were misclassified as veins. Similar measures are defined for the veins also. Table I shows the results of the classification for various classifiers. The SVM classifier gave the best performance among the four classifiers, being able to identify 97% of the arteries and 90% of the veins correctly. Misclassification of arteries as veins happened with 3% of the arteries while

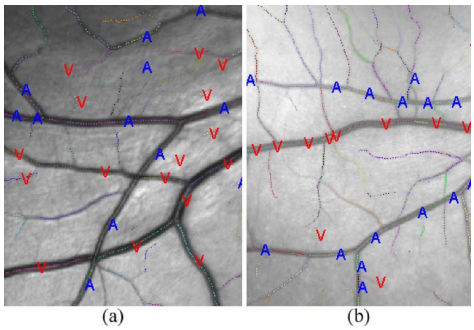

(a) (b)

Fig. 7. Sample classification results. The identified artery segments are labeled as "A" in blue and the veins are labeled as "V" in red. Vessels with small diameters are not used in the validation and hence their classification labels are not shown.

TABLE I
CLASSIFICATION RESULTS FOR DIFFERENT CLASSIFIERS. THE SVM CLASSIFIER GAVE THE BEST CLASSIFICATION PERFORMANCE WITH 97% AND 90% TRUE POSITIVE RATE FOR THE ARTERIES AND VEINS, RESPECTIVELY

Classifier	TP (Arteries)	TP (Veins)	MC (Arteries)	MC (Veins)
Nearest Neighbor	95 %	87 %	5 %	13 %
5-Nearest Neighbor	95 %	90 %	4 %	10 %
Fisher Linear Discriminant	97 %	79 %	2 %	21 %
Support Vector Machine	97 %	90 %	3 %	10 %

10% of the veins were misclassified as arteries. Fig. 7 shows the vessel classifications on two test images.

VI. DISCUSSION AND CONCLUSION

Reliable identification of arteries and vessels from retinal images can be useful in a variety of applications, such as automatic analysis of the changes in artery and vein diameters, retinal vessel oximetry and change analysis, and automatic detection of abnormalities such as branch retinal vein occlusions (BRVO). Retinal oximetry has added to the understanding of the pathophysiology of retinal disorders, including diabetic complications in the retina [57], [58] and altered oxygen delivery in glaucoma [40]. The distinguishing characteristic of BRVO is retinal ischemia in the affected areas and associated increases in vessel diameters. It was shown that diameters of occluded venules decreased after treatment of BRVO by laser photocoagulation, as did those of adjacent arteries, a response that is consistent with increased oxygen supply after renewed blood flow [59]. Thus, the vessel diameter and the oxygen status could both be used for automated detection of BRVO. A study in preterm infants using semi-automated computer analysis of digital images found that tortuosity of the retinal arteries near the optic disc varied significantly with the severity of retinopathy of prematurity (ROP) and smaller, nonsignificant increases in arterial and venular diameters were also observed [60]. The present methods will provide means to distinguish between arteries and veins and to evaluate the tortuosity and diameter changes in ROP for the two types of vessels separately.

The proposed algorithm is distinct from prior work in many ways. The proposed method is independent of the location of the retina being imaged and can work on vessels from all regions of the retina. This is distinct from prior work; for example the method described by Grisan *et al.* classifies vessels only in a well defined concentric zone around the optic disk. While many prior methods utilized only the color or intensity information [5]–[7], our method uses information from multiple wavelengths, uses structural and functional features and is fully automatic. For the reasons, the classification accuracy of our method is better than previous methods. The method described Li *et al.* uses only a structural feature, and their detection rates are approximately 83% and 90% for the arteries and veins respectively. This has to be compared with 97% and 90% in the proposed method. Grisan *et al.* reported a classification accuracy of around 88%, while the classification accuracy using the method proposed here is around 93% considering both the arteries and veins.

An interesting point to be noted is that even though the scatter plot in Fig. 5 shows a clearly linear separable case, the SVM classifier gave the best results among the four classifiers tested. The improvement in performance between the 5-NN and SVM classifier was only marginal. But we believe that for more complex data sets with large number of training points, the feature space might not be linear separable. In such a case, from a system design stand point, the use of a sophisticated mechanism such as an SVM classifier is justified to robustly classify the vessels.

Though our method works on vessels with considerable width, its success is limited on very thin vessels. This is due to the fact that as the vessel becomes thin, the central reflex is negligible and the arteries and the vessels look almost the same, hence reducing the effectiveness of the structural feature. Also, the calculation of the optical densities on very thin vessels is not stable as discussed in [4]. One possibility to classify these thin vessels is to reliably extract the vessel hierarchy from the vessel segmentation, and then assign the label of the thin vessels to the same label as that of its parent vessel (major vessel). Reliably extracting the vessel hierarchy from retinal vessels is a challenging problem. A first step in this direction was described in an earlier paper by the authors [4]. Further research is planned to extract the hierarchy from thin inter-connected vessels over large areas of the retina and to use the hierarchy information to reliably identify the vessel type for thin vessels.

ACKNOWLEDGMENT

The authors would like to thank their colleagues K. Fritzsche and C. V. Stewart of the RPI Retina team for use of the retinal vessel tracing core. L. Martinez (ITD) also assisted with data collection in these experiments.

REFERENCES

[1] T. Y. Wong, R. Klein, A. R. Sharrett, M. I. Schmidt, J. S. Pankow, D. J. Couper, B. E. K. Klein, L. D. Hubbard, and B. B. Duncan, "Retinal arteriolar narrowing and risk of diabetes mellitus in middle-aged persons," *J. Am. Med. Assoc.*, vol. 287, no. 19, pp. 2528–2533, May 2002.

[2] A. Houben, M. Canoy, H. Paling, P. Derhaag, and P. de Leeuw, "Quantitative analysis of retinal vascular changes in essential and renovascular hypertension," *J. Hypertension.*, vol. 13, pp. 1729–1733, 1995.

[3] T. Wong, R. Klein, A. Sharrett, B. Duncan, D. Couper, J. Tielsch, B. Klein, and L. Hubbard, "Retinal arteriolar narrowing and risk of coronary heart disease in men and women the atherosclerosis risk in communities study," *J. Am. Med. Assoc.*, vol. 287, no. 9, pp. 1153–1159, Mar. 2002.

[4] H. Narasimha-Iyer, J. M. Beach, B. Khoobehi, J. Ning, H. Kawano, and B. Roysam, "Algorithms for automated oximetry along the retinal vascular tree from dual-wavelength fundus images," *J. Biomed. Opt.*, vol. 10, no. 5, Oct. 2005.

[5] J. J. Yu, B. Hung, and H. Sun, "Automatic recognition of retinopathy from retinal images," in *Proc. Int. Conf. IEEE Engineering Medicine and Biology Society*, 1990, vol. 12, no. 1, pp. 171–173.

[6] K. Akita and H. Kuga, "A computer method of understanding ocular fundus images," *Pattern Recogn.*, vol. 15, no. 6, pp. 431–443, 1982.

[7] E. Grisan and A. Ruggeri, "A divide *et impera* strategy for automatic classification of retinal vessel into arteries and veins," in *Proc. 25th Annu. Int. Conf. IEEE Engineering Medicine and Biology Society*, 2003.

[8] H. Li, W. Hsu, M. L. Lee, and H. Wang, "A piecewise Gaussian model for profiling and differentiating retinal vessels," presented at the IEEE ICIP, Barcelona, Spain, Sep. 14–17, 2003.

[9] V. Mahadevan, H. Narasimha-Iyer, B. Roysam, and H. L. Tanenbaum, "Robust model-based vasculature detection in noisy biomedical images," *IEEE Trans. Inf. Technol. Biomed.*, vol. 8, no. 3, pp. 360–376, Sep. 2004.

[10] J. M. Beach, K. J. Schwenzer, S. Srinivas, D. Kim, and J. S. Tiedeman, "Oximetry of retinal vessels by dual-wavelength imaging: Calibration and influence of pigmentation," *J. Appl. Physiol.*, vol. 86, pp. 748–758, 1999.

[11] A. Hoover, V. Kouznetsova, and M. Goldbaum, "Locating blood vessels in retinal images by piecewise threshold probing of a matched filter response," *IEEE Trans. Med. Imag.*, vol. 19, no. 3, pp. 203–210, Mar. 2000.

[12] X. Jiang and D. Mojon, "Adaptive local thresholding by verification-based multithreshold probing with application to vessel detection in retinal images," *IEEETrans. Pattern Anal. Mach. Intell.*, vol. 25, no. 1, pp. 131–137, Jan. 2003.

[13] L. Zhou, M. S. Rzeszotarski, L. J. Singerman, and J. M. Chokreff, "The detection and quantification of retinopathy using digital angiograms," *IEEE Trans. Med. Imag.*, vol. 13, no. 4, pp. 619–626, 1994.

[14] R. Poli and G. Valli, "An algorithm for real-time vessel enhancement and detection," *Comput. Meth. Prog. Biomed.*, vol. 52, pp. 1–22, 1997.

[15] L. Gagnon, M. Lalonde, M. Beaulieu, and M. C. Boucher, "Procedure to detect anatomical structures in optical fundus images," *Proc SPIE*, vol. 4322, Med. Imag.: Image Process., pp. 1218–25, 2001.

[16] A. Can, H. Shen, J. N. Turner, H. L. Tanenbaum, and B. Roysam, "Rapid automated tracing and feature extraction from live high-resolution retinal fundus images using direct exploratory algorithms," *IEEE Trans. Inf. Technol. Biomed.*, vol. 3, pp. 125–138, Jun. 1999.

[17] K. Fritzsche, A. Can, H. Shen, C. Tsai, J. Turner, H. L. Tanenbuam, C. V. Stewart, and B. Roysam, "Automated model based segmentation, tracing and analysis of retinal vasculature from digital fundus images," in *Angiography and Plaque Imaging: Advanced Segmentation Techniques*, J. S. Suri and S. Laxminarayan, Eds. Boca Raton, FL: CRC Press, 2002.

[18] S. R. Aylward and E. Bullitt, "Initialization, noise, singularities, and scale in height ridge traversal for tubular object centerline extraction," *IEEE Trans. Med. Imag.*, vol. 21, no. 2, pp. 61–75, Feb. 2002.

[19] F. Zana and J. C. Klein, "Segmentation of vessel-like patterns using mathematical morphology and curvature evaluation," *IEEE Trans. Image Process.*, vol. 10, no. 7, pp. 1010–1019, Jul. 2001.

[20] T. Walter, J. C. Klein, P. Massin, and A. Erginay, "A contribution of image processing to the diagnosis of diabetic retinopathy detection of exudates in color fundus images of the human retina," *IEEE Trans. Med. Imag.*, vol. 21, no. 10, pp. 1236–1244, Oct. 2002.

[21] M. Fontaine, L. Macaire, J. G. Postaire, M. Valette, and P. Labalette, "Fundus images segmentation by unsupervised classification," in *Proc. Vision Interface*, Trois-Rivieres, QC, Canada, May 1999.

[22] J. Staal, M. D. Abramoff, M. Niemeijer, M. A. Viergever, and B. van Ginneken, "Ridge-based vessel segmentation in color images of the retina," *IEEE Trans. Med. Imag.*, vol. 23, no. 4, pp. 501–509, Apr. 2004.

[23] G. Lin, K. L. Fritzsche, C. V. Stewart, H. L. Tanenbaum, and B. Roysam, "Predictive scheduling algorithms for real-time feature extraction and spatial referencing: Application to retinal image sequences," *IEEE Trans. Biomed. Eng.*, vol. 51, no. 1, pp. 115–125, Jan. 2004.

[24] H. Shen, B. Roysam, C. V. Stewart, J. N. Turner, and H. L. Tanenbaum, "Optimal scheduling of tracing computations for real-time vascular landmark extraction from retinal fundus images," *IEEE Trans. Inf. Technol. Biomed.*, vol. 5, no. 1, pp. 77–91, Mar. 2001.

[25] S. Chaudhuri, S. Chatterjee, N. Katz, M. Nelson, and M. Goldbaum, "Detection of blood vessels in retinal images using two-dimensional matched filters," *IEEE Trans. Med. Imag.*, vol. 3, pp. 263–269, Sep. 1989.

[26] L. Gang, O. Chutatape, and S. M. Krishnan, "Detection and measurement of retinal vessels in fundus images using amplitude modified second-order Gaussian filter," *IEEE Trans. Biomed. Eng.*, vol. 49, no. 2, pp. 168–172, Feb. 2002.

[27] O. Chutatape, L. Zheng, and S. Krishnan, "Retinal blood vessel detection and tracking by matched Gaussian and Kalman filters," in *Proc. IEEE Int. Conf. Eng. Med. Biol.*, 1998, pp. 3144–3149.

[28] L. Pedersen, M. Grunkin, B. Ersboll, K. Madsen, M. Larsen, N. Christoffersen, and U. Skands, "Quantitative measurement of changes in retinal vessel diameter in ocular fundus images," *Pattern Recogn. Lett.*, vol. 21, pp. 1215–1223, 2000.

[29] K. A. Vermeer, F. M. Vos, H. G. Lemij, and A. M. Vossepoel, "A model based method for retinal blood vessel detection," *Comput. Biol. Med.*, vol. 34, no. 3, pp. 209–219, 2004.

[30] T. Pappas and J. S. Lim, "A new method for estimation of coronary artery dimensions in angiograms," *IEEE Trans. Acoust., Speech, Signal Process.*, vol. 36, no. 9, pp. 1501–1513, Sep. 1988.

[31] D. Roberts, "Analysis of vessel absorption profiles in retinal oximetry," *Med. Phys.*, vol. 14, 1987.

[32] X. Gao, A. Bharath, A. Stanton, A. Hughes, N. Chapman, and S. Thom, "A method of vessel tracking for vessel diameter measurement on retinal images," *Proc. IEEE ICIP*, pp. 881–884, 2001.

[33] J. B. Hickam, R. Frayser, and J. C. Ross, "A study of retinal venous blood oxygen saturation in human subjects by photographic means," *Circulation*, vol. 27, pp. 375–383, 1963.

[34] J. B. Hickam and R. Frayser, "Studies of the retinal circulation in man: Observations on vessel diameter, arteriovenous oxygen difference, and mean circulation time," *Circulation*, vol. 33, 1966.

[35] R. A. Laing, A. J. Cohen, and E. Friedman, "Photographic measurements of retinal blood oxygen saturation: Falling saturation rabbit experiments," *Invest. Ophthal. Vis. Sci.*, vol. 14, pp. 606–610, 1975.

[36] F. C. Delori, "Noninvasive technique for oximetry of blood in retinal vessels," *Appl. Optics*, vol. 27, pp. 1113–1125, 1988.

[37] D. Schweitzer, M. Hammer, J. Kraft, E. Thamm, E. Konigsdorffer, and J. Strobe, "*In vivo* measurement of the oxygen saturation of retinal vessels in healthy volunteers," *IEEE Trans. Biomed Engg.*, vol. 46, no. 12, pp. 1454–1465, Dec. 1999.

[38] P. K. Jensen, "Non-Invasive retinal oximetry in normal human subjects," in *Proc. Computer Assisted Fundus Image Analysis*, Turin, Italy, Mar. 28–30, 2003.

[39] M. Crittin, H. Schmidt, and C. E. Riva, "Hemoglobin oxygen saturation (SO_2) in the human ocular fundus measured by reflectance oximetry: Preliminary data in retinal veins," *Klin. Monatsbl. Augenheilkd.*, vol. 219, no. 4, pp. 289–91, 2002.

[40] B. Khoobehi, J. M. Beach, and H. Kawano, "Hyperspectral imaging for measurement of oxygen saturation in the optic nerve head," *Invest. Ophthal. Vis. Sc.*, vol. 45, no. 5, pp. 1464–1472, 2004.

[41] M. Uzumcu, F. M. Vos, A. M. Vossepoel, and G. L. van der Heijde, L. J. van Vliet, J. W. J. Heijnsdijk, T. Kielman, and P. M. W. Knijnenburg, Eds., "Theoretical analysis of a spectrophotometric technique for measuring oxygen saturation in retinal vessels," in *Proc. ASCI 2000, 6th Annu. Conf. Adv. Sch. Comp. Imag.*, Belgium, Jun. 14–16, 2000, pp. 117–121.

[42] A. Lompado, M. H. Smith, K. R. Denninghoff, and L. W. Hillman, G. H. Bearman, D. Cabib, and R. M. Levenson, Eds., "Multispectral confocal scanning laser ophthalmoscope for retinal vessel oximetry," *Proc. of SPIE (Spectral Imaging: Instrumentation, Applications, and Analysis)*, vol. 3920, , pp. 67–73, 2000.

[43] M. H. Smith, K. R. Denninghoff, L. W. Hillman, and R. A. Chipman, "Oxygen saturation measurements of blood in retinal vessels during blood loss," *J. Biomed. Opt.*, vol. 3, pp. 296–303, 1998.

[44] J. A. F. Machado, "Robust model selection and M-estimation," *Econometric Theory*, vol. 9, pp. 478–493, 1993.

[45] G. A. F. Seber and C. J. Wild, *Non-Linear Regression*. New York: Wiley, 1989, pp. 619–653.

[46] A. E. Beaton and J. W. Tukey, "The fitting of power series, meaning polynomials, illustrated on hand-spectroscopic data(with discussion)," *Technometrics*, vol. 16, pp. 147–192, 1974.

[47] P. W. Holland and R. E. Welsch, "Robust regression using iteratively reweighted least-squares," *Commu. Statist. Theory Meth.*, vol. A6, pp. 813–827, 1977.
[48] C. V. Stewart, C.-L. Tsai, and B. Roysam, "The dual-bootstrap iterative closest point algorithm with application to retinal image registration," *IEEE Trans. Med. Imag.*, vol. 22, no. 11, pp. 1379–1394, Nov. 2003.
[49] R. P. W. Duin, P. Juszczak, P. Paclik, E. Pekalska, D. de Ridder, and D. M. J. Tax, *PRTools4, A Matlab Toolbox for Pattern Recognition*. Delft, The Netherlands: Delft Univ. Technol., 2004.
[50] V. Vapnik, *Statistical Learning Theory*. New York: Wiley, 1998.
[51] M. Pontil and A. Verri, "Support vector machines for 3-D object recognition," *IEEE Trans. Pattern Anal. Mach. Intell.*, vol. 20, no. 6, pp. 637–646, Jun. 1998.
[52] V. Wan and W. M. Campbell, "Support vector machines for speaker verification and identification," in *Proc. IEEE Workshop Neural Networks for Signal Processing*, Sydney, Australia, Dec. 2000, pp. 775–784.
[53] E. Osuna, R. Freund, and F. Girosi, "Training support vector machines:Application to face detection," in *Proc. Comput. Vis. Pattern Recogn.*, Puerto Rico, 1997, pp. 130–136.
[54] T. Joachims, "Transductive inference for text classification using support vector machines," in *Proc. 16th Int. Conf. Mach. Learn.*, Bled, Slovenia, Jun. 1999, pp. 200–209.
[55] A. Schwaighofer, The SVM Toolbox for Matlab [Online]. Available: http://www.igi.tugraz.at/aschwaig/software.html
[56] V. Cherkassky and Y. Ma, "Practical selection of SVM parameters and noise estimation for SVM regression," *Neural Netw.*, vol. 17, no. 1, Jan. 2004.
[57] J. S. Tiedeman, S. E. Kirk, S. Srinivas, and J. M. Beach, "Retinal oxygen consumption during hyperglycemia in patients with diabetes without retinopathy," *Ophthal.*, vol. 105, pp. 31–36, 1998.
[58] E. Stefansson, M. B. Landers, and M. L. Wolbarsht, "Oxygenation and vasodilatation in relation to diabetic and other proliferative retinopathies," *Ophtal. Surg.*, vol. 14, pp. 209–226, 1983.
[59] A. Arnarsson and E. Stefansson, "Laser treatment and the mechanism of edema reduction in branch retinal vein occlusion," *Inves. Ophthal. Vis. Sci.*, vol. 3, pp. 877–879, 2000.
[60] C. Swanson, K. D. Cocker, K. H. Parke, M. J. Moseley, and A. R. Fielder, "Semiautomated computer analysis of vessel growth in preterm infants without and with ROP," *Br. J. Ophthal.*, vol. 87, no. 12, pp. 1474–1477, 2003.

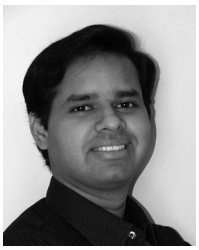

Harihar Narasimha-Iyer (S'03–M'06) received the Bachelor of Technology degree in electronics and communication engineering from the University of Kerala, India, in 2000 and the M.S. and Ph.D. degrees in electrical engineering from Rensselaer Polytechnic Institute, Troy, NY, in 2003 and 2005, respectively.

He is currently a Senior Scientist with Carl Zeiss Meditec, Dublin, CA.

His research interests include biomedical image analysis, computer vision, and pattern recognition.

Dr. Narasimha-Iyer was the recipient of the Presidential Student Award from the Microscopy Society of America and the Founders Award for Excellence from Rensselaer Polytechnic Institute, both in 2005. He is a member of the International Society for Imaging in the Eye and the Association for Research in Vision and Ophthalmology.

James M. Beach received the B.S. degree in electrical engineering and the M.S. degree in bioengineering from the University of Michigan, Ann Arbor, in 1971 and 1977, respectively. He received the Ph.D. degree in biomedical engineering from University of Virginia (UVA), Charlottesville, in 1983

He was a National Institutes of Health (NIH) Postdoctoral Fellow in the Department of Chemistry at UVA and an American Heart Fellow in the Department of Physiology. In 1993, he joined the Biomedical Engineering Department at UVA where his research focused on spectral fluorescence imaging of the microcirculation and multispectral imaging for retinal oximetry in NIH-sponsored studies of eye disease. In 2001, he moved to the Institute for Technology Development, Stennis Space Center, MS, where he continued oximetry research with hyperspectral imaging under NIH and NASA sponsorship in collaboration with the Lion's Eye Center at Louisiana State University, New Orleans, multispectral retinal imaging in collaboration with the University of Iceland and Indiana University, and automated vessel tracking with Rensselaer Polytechnic Institute, Troy, NY. He is currently Associate Professor in the Electrical and Computer Engineering Department at the University of Iceland, Reykjavik, and continues systems development for clinical retinal oximetry with OxyMap, Inc. He holds three patents.

Dr. Beach received an Innovative Instrumentation award from Instruments for Physiology and Medicine, UVA, in 1991. In 2005, he was inducted into the Space Foundation Hall of Fame as co-developer of a portable hyperspectral imaging system. He a member of Association for Research in Vision and Ophthalmology and the SPIE.

Bahram Khoobehi received the Ph.D. degree in physics from North Texas State University, Denton.

He is currently a Professor of Ophthalmology, Louisiana State University Health Sciences Center, Department of Ophthalmology, New Orleans, and also an Adjunct Associate Professor of Biomedical Engineering, at Tulane University School of Engineering, New Orleans. His research interests include hyperspectral imaging to measure oxygen saturation in the retina and optic nerve head; targeting dye and drug delivery systems to the retina; and, retinal blood flow.

Badrinath Roysam (M'89) received the B. Tech degree in electronics engineering from the Indian Institute of Technology, Madras, India, in 1984, and the M.S. and D.Sc. degrees from Washington University, St. Louis, MO, in 1987, and 1989, respectively.

He has been at Rensselaer Polytechnic Institute, Troy, NY, since 1989, where he is currently a Professor in the Electrical, Computer and Systems Engineering Department. He is an Associate Director of the Center for Subsurface Sensing and Imaging Systems (CenSSIS)—a multiuniversity NSF-sponsored engineering research center. He also holds an appointment in the Biomedical Engineering Department. His ongoing projects are in the areas of 2-D, 3-D, and 4-D biomedical image analysis, biotechnology automation, optical instrumentation, high-speed and real-time computing architectures, and parallel algorithms.

Dr. Roysam is an associate editor for the IEEE TRANSACTIONS ON INFORMATION TECHNOLOGY IN BIOMEDICINE and IEEE TRANSACTIONS ON BIOMEDICAL ENGINEERING. He is a member of IEEE, ASEE, the Microscopy Society of America, the Society for Neuroscience, the Association for Research in Vision and Ophthalmology, and the Society for Molecular Imaging.